Optik 127 (2016) 1184–1189

Contents lists available at ScienceDirect

Optik

journal homepage: www.elsevier.de/ijleo

Framelet-based sparse regularization for uneven intensity correction of remote sensing images in a retinex variational framework

Xia Lan [a], Zhiyong Zuo [a,*], Huanfeng Shen [b], Liangpei Zhang [c], Jing Hu [d]

[a] The 10th Institute of China Electronics Technology Group Corporation, Chengdu 610036, China
[b] The School of Resource and Environmental Sciences, Wuhan University, Wuhan 430079, China
[c] The State Key Laboratory of Information Engineering in Surveying, Mapping, and Remote Sensing, Wuhan University, Wuhan 430079, China
[d] National Key Laboratory of Science and Technology on Multispectral Information Processing, Institute for Pattern Recognition and Artificial Intelligence, Huazhong University of Science and Technology, Wuhan 430074, China

ARTICLE INFO

Article history:
Received 4 February 2015
Accepted 29 October 2015

Keywords:
Framelet
Retinex
Uneven intensity correction
Remote sensing image
Split Bregman algorithm

ABSTRACT

Correcting uneven intensity distribution from a single image has long been a challenging problem with remote sensing image. In this paper, an analysis-based sparse prior is employed in the retinex variational framework for the uneven intensity correction of remote sensing images. This sparse regularization model is used to adjust uneven intensity by regularizing the sparsity of the reflectance component under framelet transform. Furthermore, the alternating minimization algorithm and split Bregman method are adopted to solve the framelet-based sparse regularization model. The experiments, with both simulated images and real-life images, show that the proposed model can effectively correct the uneven intensity distribution.

1. Introduction

Uneven intensity distribution exists in most remote sensing images. However, the remote sensing images are very important for the subsequent image processing, i.e., change detection, image classification, and other applications [15,16]; thus, it is extremely important to correct the uneven intensity.

In order to overcome the drawback of absolute radiometric correction, many relative radiometric correction algorithms have been developed to adjust the uneven intensity distribution. The homomorphic filter (HF) and histogram equalization (HE) are the popular approaches used to adjust the uneven illumination and redistribute the intensity distribution [5,19]. According to retinex theory [9], a number of retinex-based models are utilized to correct the uneven intensity [6,11,12,14]; besides, some retinex variational models have also been applied in this field [7,10,13]. Kimmel et al. [7] proposed a L2 regularized model for the illumination component to indirectly obtain the reflectance. Li et al. [10] provided a joint L2 and TV regularized model for the reflectance component. Michael et al. [13] used the L2 regularized term of the illumination and the TV regularized term of the reflectance. Although great advances have been made, there is still room for improvement.

It is well known that most images have a sparse approximation. Thus, in recent years, the sparsity-based prior has been a common choice for the regularization term [3], and has been widely used in the fields of denoising [4], deblurring [3], super-resolution [18], and so on. There are two typical sparse priors, namely, the synthesis-based and analysis-based sparse priors [3]. These priors are based on the fact that natural images usually be represented or approximated sparsely in some redundant transformed domain, such as wavelet, framelet, etc. In this paper, the analysis-based sparse prior regularization is adopted to correct the uneven intensity in the retinex variational framework. Since the reflectance component can be approximated sparsely, this sparse regularization model is used to adjust the uneven intensity by regularizing the sparsity of the reflectance component under tight frame system. For its efficiency and simplicity, the framelet tight frame system is selected to approximate the reflectance component. Moreover, the split Bregman algorithm is used to solve the proposed model, i.e., the framelet-based sparse regularization model in retinex variational framework.

The rest of this paper is organized as follows. In Section 2, we review the analysis-based sparse prior regularization and the framelet system. Section 3 presents the proposed framelet-based uneven intensity correction model and the split

* Corresponding author. Tel.: +86 18109064295.
E-mail address: zzy.iprai@gmail.com (Z. Zuo).

http://dx.doi.org/10.1016/j.ijleo.2015.10.214
0030-4026/

Bregman algorithm is used to solve it. The experiment results are presented in Section 4. Section 5 provides the conclusion.

2. The analysis-based sparse prior the framelet system

In this section, a brief review of the analysis-based sparse prior is given. First, we denote the observed image g as the lexicographically ordered column vector in $\mathbb{R}^n$, and $W \in \mathbb{R}^{m\times n}$ is an analysis operator. The data $g \in \mathbb{R}^n$ can be transformed to some coefficients $Wg \in \mathbb{R}^m$ by the analysis operator W. In general, W is a redundant transform operator, where $m > n$.

When the analysis-based prior is used for the regularization model, the goal is to look for the most sparse solution among the transform coefficient vectors (the coefficients Wg decomposed by the analysis operator W) [3]. In the different application fields, different analysis operators can be used to regularize the data. Thus, it is important to choose a suitable redundant transform, e.g., a tight frame system. In this paper, a piecewise linear B-spline tight frame is used, which is derived by using the piecewise linear B-spline function as the refinable function [3]. The framelet is as follows [2,3]:

$$h_0 = \frac{1}{4}[1, 2, 1]; \quad h_1 = \frac{\sqrt{2}}{4}[1, 0, -1]; \quad h_2 = \frac{1}{4}[-1, 2, -1] \tag{1}$$

In the numerical computation, the wavelet frame transform can be represented by the decomposition matrix W, which is constructed depending on the boundary condition. The complete generating procedure of the matrix is presented in [2,3]. With the decomposition matrix, the data g can be transformed to the frame coefficient vector

$$t = Wg \tag{2}$$

The reconstruction algorithm W^* is the inverse transform of W, as shown

$$g = W^* t \tag{3}$$

where $W^*W = I$. Generally speaking, $WW^* \neq I$ unless W is an orthonormal basis.

3. The proposed framelet-based sparse regularization model

3.1. The proposed model

The proposed model belongs to the retinex variational framework. According to retinex theory, image intensity is composed of two factors: illumination and reflectance. In the spatial domain, the product of these two components forms the image intensity, i.e.,

$$S(x) = L(x) \cdot R(x) \tag{4}$$

In order to facilitate computation, the product form (4) is converted to the logarithmic domain, i.e.,

$$s = l + r \tag{5}$$

where s, l, and r are equal to $\log(S)$, $\log(L)$, and $\log(R)$, respectively. $S(x)$, $L(x)$, and $R(x)$, respectively, represent the observed image intensity, the natural illumination and the object reflectance, which depends on the physical characteristics of the object materials [10]. x is the pixel location in the image. In (4), the reflectance component is normalized as $0 \le R \le 1$, owing to its natural characteristics [10,13]. Thus, we can get the constraints $r \le 0$ and $l \ge s$. The relationship (4) between these three variables is still valid for each channel of the multiband image [10].

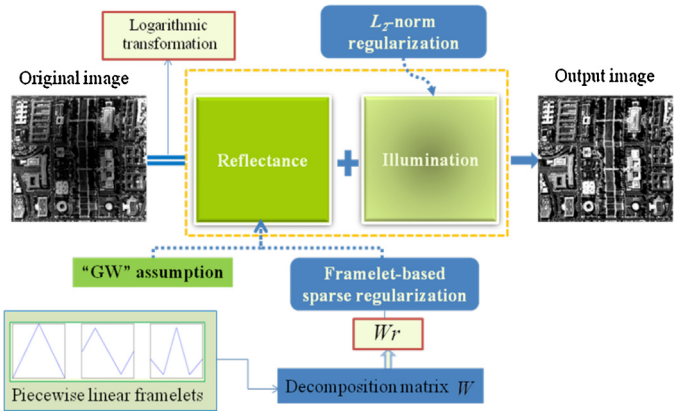

Fig. 1. The main procedure of the proposed method.

Our goal is to solve the reflectance component r from (5). In this paper, we propose a framelet-based sparse regularized variational model to correct the uneven intensity distribution. There are four terms in this variational model. The first term, the data fidelity term $||s - l - r||_2^2$, is used to preserve data consistency, where $||\cdot||_2$ denotes the L_2-norm. The use of the data fidelity term can ensure that the reflectance component does not deviate from the observed value. Secondly, according to the "gray world" (GW) assumption [1,10], the average color intensity in a scene is perceived as the middle gray intensity. Thus, in the logarithmic domain, this constraint term is translated as $[\exp(r) - 0.5]^2$.

It is well known that a regularized prior term is important for a variational model. Next, we introduce two regularized prior terms for illumination and reflectance, respectively. According to the characteristics of natural illumination, the illumination component l is spatially smooth. In the proposed model, the regularization term $||\nabla l||_2^2$ is used to preserve the continuity of the illumination component.

Finally, the most important task is to choose the regularization prior for the reflectance. Since the reflectance component r can be approximated sparsely, the sparse regularization term is used to adjust the uneven intensity by regularizing the sparsity of the reflectance component r under framelet system. When this sparse prior of the reflectance is used in the variational model, it can alleviate the distortion caused by the uneven illumination and can preserve the information of the intensity and structure. Thus, the analysis-based sparse regularization term is employed, as shown:

$$\text{sparse prior}: \ ||Wr||_1 \tag{6}$$

where W is the framelet transform introduced in the last section. Here, $||\cdot||_1$ denotes the L_1-norm. Summarizing the above analysis, the main procedure is shown in Fig. 1.

Finally, we give the framelet-based sparse regularized variational model in the retinex variational framework, as follows:

$$\min F(r, l) = \sum_{\Omega} \left\{ \left\|s - l - r\right\|_2^2 + \lambda_1 \left\|Wr\right\|_1 + \lambda_2 \left\|\nabla l\right\|_2^2 + \alpha[\exp(r) - 0.5]^2 \right\} \quad \text{s.t.} \quad r \le 0, \ l \ge s \tag{7}$$

where the positive parameters λ_1, λ_2, and α are used to trade off each term in the proposed model.

3.2. Numerical algorithms

In this section, our aim is to look for the solution to the proposed model (7). Since two unknown variables r and l are involved in the proposed model, the alternating minimization algorithm is adopted [13]. The alternating minimization scheme (Algorithm 1)

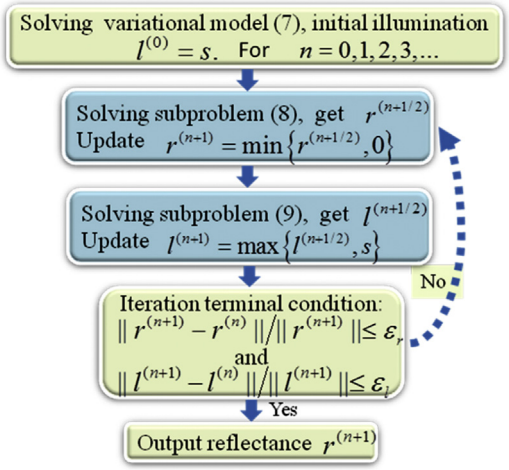

Fig. 2. The alternating minimization scheme (Algorithm 1).

is described in Fig. 2. In Fig. 2, the two subproblems are shown as follows:

$$r^{(n+1/2)} = \arg\min_r \sum_\Omega \left\{ \left\| s - l^{(n)} - r \right\|_2^2 + \alpha[\exp(r) - 0.5]^2 + \lambda_1 \left\| Wr \right\|_1 \right\} \tag{8}$$

$$l^{(n+1/2)} = \arg\min_l \sum_\Omega \left[\left\| s - l - r^{(n+1)} \right\|_2^2 + \lambda_2 \left\| \nabla l \right\|_2^2 \right] \tag{9}$$

The next task is to solve the above subproblems. For the first subproblem (8), since the L_1-norm term $\|Wr\|_1$ is nonseparable, it is difficult to solve this sparsity-based regularization term. In order to overcome this difficulty, the split Bregman algorithm is used to solve this difficult problem [3]. According to the split Bregman algorithm, the subproblem (8) is equal to the following constrained problem by adding in a new auxiliary variable d:

$$\arg\min_{r,d} \sum_\Omega \left\{ \left\| s - l^{(n)} - r \right\|_2^2 + \alpha[\exp(r) - 0.5]^2 + \lambda_1 \left\| d \right\|_1 \right\} \quad s.t. \quad d = Wr \tag{10}$$

This problem is then converted to a unconstrained minimization problem, i.e.,

$$\arg\min_{r,d} \sum_\Omega \left\{ \left\| s - l^{(n)} - r \right\|_2^2 + \alpha[\exp(r) - 0.5]^2 + \lambda_1 \left\| d \right\|_1 + \lambda \left\| d - Wr - b \right\|_2^2 \right\} \tag{11}$$

where b is the Bregman iteration parameter, and λ is a positive parameter. The detailed procedure is as follows:

Step 1. Set $v^{(0)} = 0$ and $b^{(0)} = 0$. For $i = 0, 1, 2, 3, \ldots$,
Step 2. At the ith iteration, given $v^{(i)}$ and $b^{(i)}$, update $d^{(i+1)}$ by the following:

$$d^{(i+1)} = T_{\lambda_1/(2\lambda)}(Wv^{(i)} + b^{(i)}) \tag{12}$$

where $T_\cdot(\cdot)$ is the soft thresholding operator [3].

And then, compute $v^{(i+1)}$ by solving the differentiable optimization problem as follow:

$$\arg\min_v \sum_\Omega \left\{ \left\| s - l^{(n)} - v \right\|_2^2 + \alpha[\exp(v) - 0.5]^2 + \lambda \left\| d^{(i+1)} - Wv - b^{(i)} \right\|_2^2 \right\} \tag{13}$$

For solving (13), it becomes

$$v^{(i+1)} = (1+\lambda)^{-1}\{(s - l^{(n)}) - \alpha \exp(v^{(i)})[\exp(v^{(i)}) - 0.5] + \lambda W^*(d^{(i+1)} - b^{(i)})\} \tag{14}$$

where W^* is the inverse transform of W, which is described in Section 2. Both the Fourier transformation and the Gauss–Seidel method are valid for the above problem.

Last, update $b^{(i+1)}$ by the following

$$b^{(i+1)} = b^{(i)} - (d^{(i+1)} - Wv^{(i+1)}) \tag{15}$$

Step 3. Let $r^{(n+1/2)} = v^{(i+1)}$ until $(\|v^{(i+1)} - v^{(i)}\|)/v^{(i+1)} \le \varepsilon_v$

The last task is to solve the second subproblem (9). Since this is a differentiable optimization problem, it is easy to look for its solution. The detailed iterative algorithm is as follows:

$$l^{(n+1/2)} = (\lambda_2 \nabla^* \nabla + I)^{-1}(s - r^{(n+1)}) \tag{16}$$

To solve (16), we can use the Fourier transformation and the Gauss–Seidel method. At this point, the two subproblems have been solved, i.e., Algorithm 1 is complete.

In this section, the proposed framelet-based uneven intensity correction model (7) is solved by the alternating minimization algorithm and the split Bregman method. Finally, the reflectance component r is obtained from the uneven intensity distribution. Since this reflectance component r is in the logarithmic domain, it should be transformed to the reflectance in the spatial domain, which is what we require.

4. Experiments and discussion

In this section, simulated and real data are used to verify the proposed method. We compare the proposed method with the Li's method [10] and Michael's method [13]. In order to give an overall assessment, several quantitative indexes are adopted, including evaluating the gray value similarity and the structural similarity. For the simulated experiments, four different quantitative indexes (PSNR [2,10,17], MSE [10], SSIM [20], GSIM [8]) based on the reference data are employed to assess the proposed method. For the real-life experiments, since clear images are hard to obtain, the above full-reference evaluation indexes are invalid. Thus, the Q-metric [17], which is based on the non-reference image, is employed to assess the performance of the proposed method. The smaller the value of MSE, the better the image quality, and the larger the values of other indexes, the better the performance.

4.1. Simulated data

Two data sets are chosen to verify the efficacy and robustness of the proposed method: the "Wuhan" (in China) image of size 200×200 in Fig. 3a and the "Washington" image of size 307×280 in Fig. 3b, which were acquired by Landsat TM and the HYDICE sensors, respectively. For each data set, four different simulated illuminations are applied, which results in four different cases of degradation. Here, to save space, we only provide the four simulated cases for the Washington image: horizontal, vertical, Gaussian-I, and Gaussian-II degradation, as shown in Fig. 4c–f. For the Wuhan image, the same degradation is simulated.

The quantitative evaluation results for the Wuhan and Washington images are shown in Tables 1 and 2, respectively. From

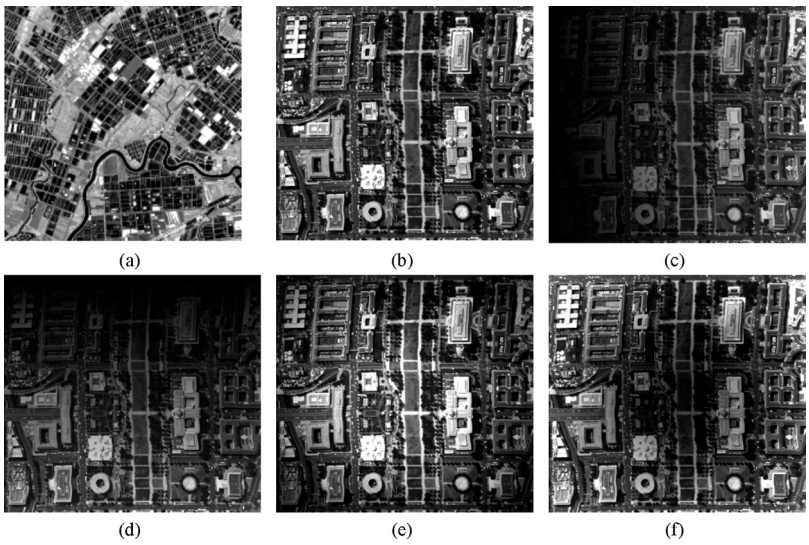

Fig. 3. The original data sets and the four degradation cases. (a) Wuhan image. (b) Washington, DC image. (c) Horizontal. (d) Vertical. (e) Gaussian-I. (f) Gaussian-II.

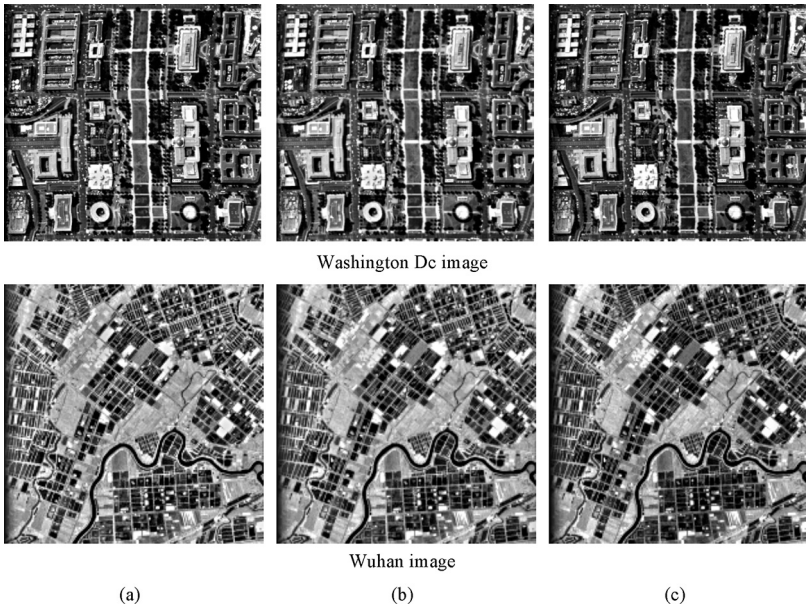

Fig. 4. The comparison results of the horizontal degradation. (a) Li's. (b) Michael's. (c) Frame.

Table 1
The quantitative evaluation results for the Wuhan image.

Type	Method	PSNR	MSE	SSIM	GSIM
Horizontal	Li's	21.15	499.38	0.9525	0.9916
	Michael's	22.55	361.24	0.9671	0.9935
	Frame	**24.22**	**246.09**	**0.9810**	**0.9952**
Vertical	Li's	20.97	519.52	0.9529	0.9916
	Michael's	22.23	389.11	0.9649	0.9936
	Frame	**24.14**	**250.87**	**0.9839**	**0.9953**
Gaussian-I	Li's	22.12	399.30	0.9552	0.9933
	Michael's	24.20	247.25	0.9785	0.9969
	Frame	**25.61**	**178.78**	**0.9823**	**0.9972**
Gaussian-II	Li's	22.62	355.63	0.9621	0.9941
	Michael's	24.96	207.47	0.9802	0.9968
	Frame	**26.22**	**155.42**	**0.9868**	**0.9978**

Table 2
The quantitative evaluation results for the Washington image.

Type	Method	PSNR	MSE	SSIM	GSIM
Horizontal	Li's	23.36	300.28	0.9613	0.9920
	Michael's	24.41	235.78	0.9645	0.9932
	Frame	**25.36**	**189.47**	**0.9765**	**0.9956**
Vertical	Li's	24.84	213.17	0.9696	0.9942
	Michael's	25.72	174.41	0.9734	0.9953
	Frame	**26.40**	**149.13**	**0.9798**	**0.9963**
Gaussian-I	Li's	23.41	296.57	0.9609	0.9931
	Michael's	24.43	234.62	0.9704	0.9945
	Frame	**25.48**	**184.16**	**0.9783**	**0.9961**
Gaussian-II	Li's	23.76	273.27	0.9560	0.9914
	Michael's	25.26	193.69	0.9671	0.9937
	Frame	**26.40**	**148.83**	**0.9740**	**0.9961**

the comparison of the results, it can be clearly seen that the proposed method provides a better result than the other methods; it provides the lowest MSE and the highest PSNR, SSIM, and GSIM values, which demonstrates that the proposed method provides a good representation of the original clear image, both in terms of gray intensity and structure information. This is because that the data fidelity term is used, i.e., gray-intensity close to the original clear image intensity in the proposed

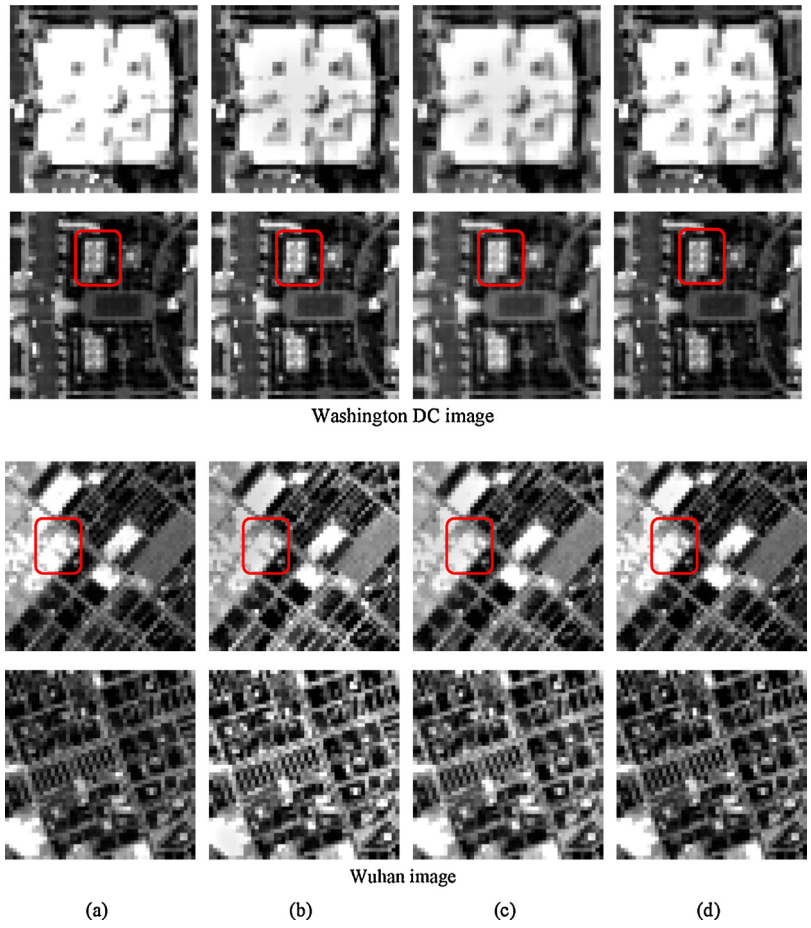

Fig. 5. Detailed regions cropped from the original image Figs. 3a,b and 4. (a) Original. (b) Li's. (c) Michael's. (d) Frame.

model. Furthermore, the most important point is the use of the framelet-based sparse regularization, which enforces the sparse constraint of the reflectance and preserves the structure information.

In order to further confirm the effectiveness of the proposed method, visual comparison results are provided. The comparison results for the horizontal degradation case are shown in Fig. 4. To clearly display the comparative visual results, detailed regions from Fig. 4 are shown in Fig. 5. From the detailed region comparison in Fig. 5, it can be seen that the frame-based method can effectively preserve the information of intensity and structure close to the original image, which is consistent with the quantitative assessment results in Tables 1 and 2. Thus, in terms of both the visual comparison and objective assessment, the proposed method outperforms the other methods.

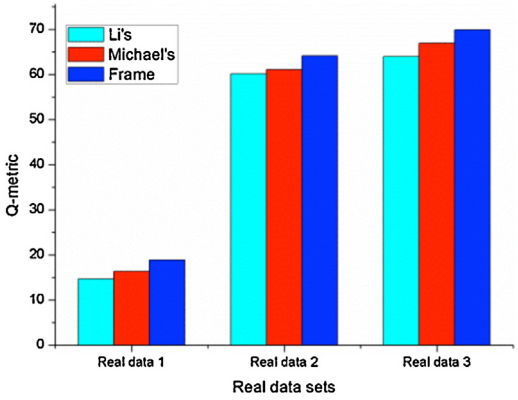

Fig. 6. The histogram of the comparative results using the Q-metric.

4.2. Real data

To further illustrate the efficacy of the proposed method, we also carry out experiments on three real data sets, which are from [10]. The quantitative assessment results using the Q-metric index for these three real data sets are shown in Fig. 6. From the Q-metric histogram, it can be seen that the proposed method provides the highest Q-metric value, which indicates that the proposed method is better than the other methods. Here, to save space, we do not show all the visual results. One of the three data sets and the corresponding restored results by the proposed method are shown in Fig. 7.

Fig. 7. The results for the real data sets. (a) Real data 1. (b) The adjusted result of real data 1 by the proposed method.

5. Conclusions

In this paper, we present a framelet-based sparse regularized variational model to adjust uneven intensity distribution in remote sensing image. In this model, since the reflectance component has a sparse approximation, a sparse prior is chose as the regularization term for the reflectance. The alternating minimization algorithm and split Bregman method are used to solve the framelet-based sparse regularized variational model. Based on both the visual effect and the quantitative assessment, extensive experiments demonstrate that the proposed method is better than Li's model and Michael's model.

Acknowledgments

This work was supported in part by the National Basic Research Program of China (973 Program) under Grant 2011CB707105, the National Natural Science Foundation of China under Grants Nos. 41271376, 60736010, 60902060, and 61227007, Hubei Natural Science Foundation under Grant 2011CDA096, Program for Changjiang Scholars and Innovative Research Team in University (IRT1278).

References

[1] R.P. Amestoy, E. Provenzi, M. Bertalmío, V. Caselles, A perceptually inspired variational framework for color enhancement, IEEE Trans. Pattern Anal. Mach. Intell. 31 (2009) 458–474.
[2] J.F. Cai, R.H. Chan, Z. Shen, A framelet-based image inpainting algorithm, Appl. Comput. Harmon. Anal. 24 (2008) 131–149.
[3] J.F. Cai, H. Ji, C. Liu, Z. Shen, Framelet-based blind motion deblurring from a single image, IEEE Trans. Image Process. 21 (2012) 562–572.
[4] M. Elad, M. Aharon, Image denoising via sparse and redundant representations over learned dictionaries, IEEE Trans. Image Process. 15 (2006) 3736–3745.
[5] R.C. Gonzalez, R.E. Woods, Digtal Image Processing, 3rd ed., Prentice-Hall, NJ, 2007.
[6] D.J. Jobson, Z.-u. Rahman, G.A. Woodell, Properties and performance of a center/surround retinex, IEEE Trans. Image Process. 6 (1997) 451–462.
[7] R. Kimmel, M. Elad, D. Shaked, R. Keshet, I. Sobel, A variational framework for retinex, Int. J. Comput. Vis. 52 (2003) 7–23.
[8] A. Liu, W. Lin, M. Narwaria, Image quality assessment based on gradient similarity, IEEE Trans. Image Process. 21 (2012) 1500–1512.
[9] E.H. Land, J.J. McCann, Lightness and retinex theory, J. Opt. Soc. Am. 61 (1971) 1–11.
[10] H. Li, L. Zhang, H. Shen, A perceptually inspired variational method for the uneven intensity correction of remote sensing images, IEEE Trans. Geosci. Remote Sens. 50 (2012) 3053–3065.
[11] J.M. Morel, A.B. Petro, C. Sbert, A PDE formalization of retinex theory, IEEE Trans. Image Process. 19 (2010) 2825–2837.
[12] W. Ma, J.M. Morel, S. Osher, A. Chien, An L1-based variational model for Retinex theory and its application to medical images, in: IEEE Conference on Computer Vision and Pattern Recognition (CVPR), 2011, pp. 153–160.
[13] M.K. Ng, W. Wang, A total variation model for retinex, SIAM J. Imaging Sci. 4 (2011) 345–365.
[14] Z.-U. Rahman, D.J. Jobson, G.A. Woodell, Retinex processing for automatic image enhancement, J. Electron. Imaging 13 (2004) 100–110.
[15] A. Singh, Review article. Digital change detection techniques using remotely-sensed data, Int. J. Remote Sens. 10 (1989) 989–1003.
[16] C. Song, C.E. Woodcock, K.C. Seto, M.P. Lenney, S.A. Macomber, Classification and change detection using Landsat TM data: when and how to correct atmospheric effects? Remote Sens. Environ. 75 (2001) 230–244.
[17] H. Shen, L. Du, L. Zhang, W. Gong, A blind restoration method for remote sensing images, IEEE Geosci. Remote Sens. Lett. 9 (2012) 1137–1141.
[18] J. Yang, J. Wright, T.S. Huang, Y. Ma, Image super-resolution via sparse representation, IEEE Trans. Image Process. 19 (2010) 2861–2873.
[19] M.F. Zakaria, H. Ibrahim, S.A. Suandi, A review: image compensation techniques, in: 2nd International Conference on Computer Engineering and Technology, vol. 7, 2010, pp. 404–408.
[20] X. Lan, Z.Y. Zuo, Random-valued impulse noise removal by the adaptive switching median detectors and detail-preserving regularization, Optik 125 (2014) 1101–1105.